Biogeosciences, 9, 179–191, 2012
www.biogeosciences.net/9/179/2012/
doi:10.5194/bg-9-179-2012

Biogeosciences

Mapping tropical forest biomass with radar and spaceborne LiDAR in Lopé National Park, Gabon: overcoming problems of high biomass and persistent cloud

E. T. A. Mitchard[1], S. S. Saatchi[2], L. J. T. White[3,4,5], K. A. Abernethy[4,5], K. J. Jeffery[3,4,5], S. L. Lewis[6,10], M. Collins[7], M. A. Lefsky[8], M. E. Leal[9], I. H. Woodhouse[1], and P. Meir[1]

[1]School of GeoSciences, University of Edinburgh, EH8 9XP, UK
[2]Jet Propulsion Laboratory, California Institute of Technology, Pasadena, California, USA
[3]Agence Nationale des Parcs Nationaux, Libreville, Gabon
[4]School of Natural Sciences, University of Stirling, Stirling, FK9 4LA, UK
[5]Institut de Recherche en Ecologie Tropicale, CENAREST, Libreville, Gabon
[6]Earth and Biosphere Institute, School of Geography, University of Leeds, UK
[7]Grantham Research Institute on Climate Change and the Environment, London School of Economics, London, UK
[8]Natural Resource Ecology Laboratory, Colorado State University, Fort Collins, Colorado, USA
[9]Missouri Botanical Garden, St. Louis, Missouri, USA
[10]Department of Geography, University College London, London, UK

Correspondence to: E. T. A. Mitchard (edward.mitchard@ed.ac.uk)

Received: 23 April 2011 – Published in Biogeosciences Discuss.: 29 August 2011
Revised: 20 December 2011 – Accepted: 21 December 2011 – Published: 10 January 2012

Abstract. Spatially-explicit maps of aboveground biomass are essential for calculating the losses and gains in forest carbon at a regional to national level. The production of such maps across wide areas will become increasingly necessary as international efforts to protect primary forests, such as the REDD+ (Reducing Emissions from Deforestation and forest Degradation) mechanism, come into effect, alongside their use for management and research more generally. However, mapping biomass over high-biomass tropical forest is challenging as (1) direct regressions with optical and radar data saturate, (2) much of the tropics is persistently cloud-covered, reducing the availability of optical data, (3) many regions include steep topography, making the use of radar data complex, (5) while LiDAR data does not suffer from saturation, expensive aircraft-derived data are necessary for complete coverage.

We present a solution to the problems, using a combination of terrain-corrected L-band radar data (ALOS PALSAR), spaceborne LiDAR data (ICESat GLAS) and ground-based data. We map Gabon's Lopé National Park (5000 km^2) because it includes a range of vegetation types from savanna to closed-canopy tropical forest, is topographically complex, has no recent contiguous cloud-free high-resolution optical data, and the dense forest is above the saturation point for radar. Our 100 m resolution biomass map is derived from fusing spaceborne LiDAR (7142 ICESat GLAS footprints), 96 ground-based plots (average size 0.8 ha) and an unsupervised classification of terrain-corrected ALOS PALSAR radar data, from which we derive the aboveground biomass stocks of the park to be 78 Tg C (173 Mg C ha^{-1}). This value is consistent with our field data average of 181 Mg C ha^{-1}, from the field plots measured in 2009 covering a total of 78 ha, and which are independent as they were not used for the GLAS-biomass estimation. We estimate an uncertainty of ±25 % on our carbon stock value for the park. This error term includes uncertainties resulting from the use of a generic tropical allometric equation, the use of GLAS data to estimate Lorey's height, and the necessity of separating the landscape into distinct classes.

As there is currently no spaceborne LiDAR satellite in operation (GLAS data is available for 2003–2009 only), this methodology is not suitable for change-detection. This research underlines the need for new satellite LiDAR data to provide the potential for biomass-change estimates, although this need will not be met before 2015.

Published by Copernicus Publications on behalf of the European Geosciences Union.

1 Introduction

Tropical forest ecosystems have a variety of values, monetary and otherwise, that vary markedly with the scale considered. However, many of these, especially the more general benefits at a larger scale, are often not included in decisions relating to whether a forest area remains forest or is converted to another land-use (Stern, 2008; Engel et al., 2008). At a local scale the individual plants and animals have value, providing non-timber forest products, bushmeat, fuel, and timber (Ahrends et al., 2010); at a regional scale they can provide protection from extreme weather events and preserve water supplies (Kaiser and Roumasset, 2002; Swetnam et al., 2011); and at a global scale they influence global energy budgets through regulation of evapotranspiration, rainfall, and other climatic variables (Meir et al., 2006), also acting as a large store of carbon, and as a carbon sink (Phillips et al., 2008; Lewis et al., 2009a; Lewis et al., 2009b). The fate of an area of forest has tended to be controlled by the opportunity to liquidate its considerable timber value (Geist and Lambin, 2002) by destructively harvesting its trees, or clearing the land to convert it to a more productive land-use, e.g. agriculture (though in many cases local people derive no benefit from conversion (Rodrigues et al., 2009)). Further difficulties arise in the optimum allocation of land to differing uses due to ownership, sovereignty, governance, and the ability and will to monitor forests, particularly at larger scales (Chhatre and Agrawal, 2008, 2009).

One approach to preventing this loss of forests has been attempts to place a price on forests, based on the carbon they store, with the avoided emissions from deforestation producing carbon credits tradable on carbon markets. Carbon is only one element of the benefits provided by living forests, but it is one that is relatively tangible and easy to quantify. Past international structures largely excluded pricing existing forest carbon, for example under the United Nations Clean Development Mechanism (CDM), which formed part of the Kyoto Treaty, carbon credits for forestry were given only for planting new forests or for reforestation, rather than for protecting threatened forests. However, the 2010 Cancun Agreement, agreed at the UNFCCC COP-16 Conference, has created an international framework for valuing forest carbon within the Reducing Emissions from Deforestation and forest Degradation (REDD+) scheme. The aim is to rapidly and radically reduce the rate of deforestation across the tropics, via performance-related payments to countries that reduce deforestation and degradation related carbon emissions (Clements, 2010). Though the details of REDD+ are yet to be finalised, its adoption was agreed at COP16 at Cancun, and considerable funds have already been committed (USD 28.3 billion have been committed by the developed world to developing world as fast-start finance for climate mitigation programs, including REDD+ (WRI, 2010)). Additionally, REDD+ transfers through government-government agreements and through the voluntary sector have already started, and are accelerating (Clements et al., 2010).

Whilst recognising the numerous limitations and problems associated with valuing forests for their carbon alone, a carbon price may establish a minimum value for forests, which may alter the decisions of land-owners in the future. Yet such a price associated with an area of forest can only be assessed if the carbon stocks of an area of forest can be accurately determined, with known uncertainties giving a minimum carbon stock at each time point, and then such a carbon map updated regularly in order to calculate deforestation rates, and therefore payments.

Scientific forest inventory plots are thought to provide the most accurate data on the aboveground biomass (AGB) of an area: these usually involve measuring the diameter at breast height (DBH), and ideally the height and species too, of every tree with a DBH >10 cm (Brown, 1997; Phillips et al., 2009). AGB is then estimated from these measurements using either locally-derived or standard allometric equations; there are thought to be significant errors associated with these equations, as destructive harvesting data is not available for specific species and areas. Often for tropical forests a pantropical equation is used, derived from 2410 destructively harvested trees from 27 sites (Chave et al., 2005). This study includes equations stratified by forest type, with DBH, height and wood density as parameters: this approach not only reduces the model error compared with using DBH alone, but also increases applicability to tree-types not used to define the original equations.

However, for reasons of resources, time and access, it is not possible to place a sufficient number of plots across a forested area, let alone a country, in order to be able to use such plots to estimate AGB for the whole area directly. Instead remote sensing data is used to extrapolate the plot data across the landscape, with the methods used split into two major categories:

1. Direct statistical relationship between AGB and a remote sensing variable (or variables, possibly including modelled variables and environmental data layers), allowing the production of a continuous AGB map for the area. With the notable exception of LiDAR (see below), such relationships are strong for lower AGB levels but tend to decrease in accuracy and eventually saturate as AGB increases, making higher biomass areas hard to map. This saturation point varies greatly depending both on the source data and vegetation type – ranging from 15–70 $\mathrm{Mg\,ha^{-1}}$ for visible/near-infrared vegetation indices (Lu, 2006), or from 40 to 150 $\mathrm{Mg\,ha^{-1}}$ for L-band radar data (Lu, 2006; Mitchard et al., 2009).

2. Classification into landcover type, usually using optical remote sensing data, with each forest type then given an AGB value and these classes then summed to estimate AGB over the whole site. Ideally the average

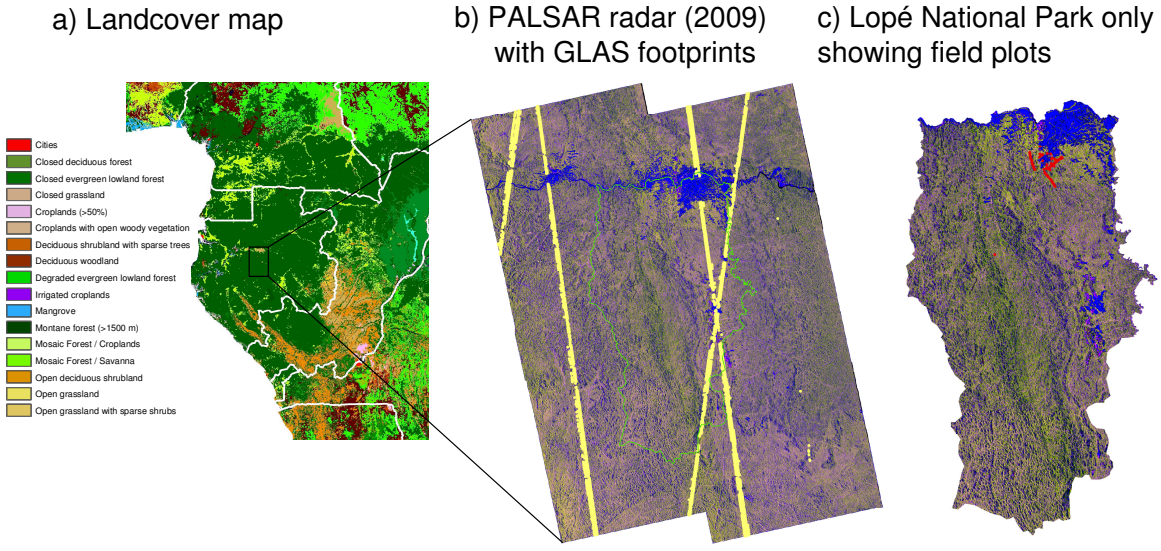

Fig. 1. **(a)** Map showing the location of the field site within a landcover map for the year 2000 (Mayaux et al., 2004), **(b)** Phased-Array L-band Synthetic Aperture Radar (PALSAR) mosaic (HH in red, HV in green, and HH/HV in blue) shown with the location of Geoscience Laser Altimeter System (GLAS) LiDAR footprints, after cloud- and slope- filtering, **(c)** the same radar image, but cut out around Lopé National Park, showing the location of the field plots.

AGB of each class is derived from field data, but often national or continental average values are used (GOFC-GOLD, 2009).

An exception to the above is LiDAR data, which by sending a short pulse of laser light either from an aircraft or from space can be used to elucidate the height and even vertical structure of a forest. Tree height, and other LiDAR-derived metrics, have been shown to relate strongly to forest biomass, with no saturation at higher biomass values (Lefsky et al., 2005). Unfortunately aircraft LiDAR data acquisition is costly, and the capacity to collect annual data over whole countries does not exist currently. However, space-borne LiDAR data was collected by the ICESat sensor from 2003 to 2009 (Lefsky, 2010), and more such data will be collected by ICESat 2 (Abdalati et al., 2010), due for launch in 2015. Aircraft LiDAR tends to be imaging LiDAR, with small footprints collected at a very high density, leading to a detailed 3-dimensional image of the area of interest; however current spaceborne systems are profiling LiDARs, collecting isolated, widely separated footprints, thus sampling the landscape. As a result in order to create full-coverage spatial layers from spaceborne LiDAR the data must be fused with other datasets. It has been shown previously that satellite LiDAR data has great potential for estimating biomass over large areas when fused with radar data (Shugart et al., 2010).

Methods for estimating AGB using the methods above are relatively well established, and have been employed as part of the monitoring schemes for many pilot REDD+ projects (CCBA, 2011), principally involving the classification approach given as 2) above. However, much of the tropics is suboptimal for the above methods in three respects. Firstly, many areas exhibit frequent cloud-cover, making classification using optical data from a single time-point next to impossible. Secondly, many areas include high biomass forest, at which most direct AGB-estimation methods saturate. Third, many forest overlay areas of steep topography, making radar data less useful. Thus methods to overcome these obstacles are needed: this paper aims to demonstrate a new methodology for overcoming these problems.

Here we use the mountainous and persistently cloud-covered Lopé National Park in Gabon to show how a novel AGB estimation method, involving terrain-corrected L-band radar data, field data and GLAS LiDAR data, can accurately determine AGB over a densely forested landscape with specified and relatively high accuracy. The use of high resolution optical data was not possible over this site, as there are no cloud-free SPOT, ASTER or Landsat scenes covering over 50 % of the study site from 2000 to the present day.

2 Study site

The study area is the Lopé National Park (LNP), which is situated in central Gabon (Fig. 1), and covers an area of 4948 km^2; it has been a wildlife reserve since 1946, and a National Park since 2002. Though surrounded by closed-canopy tropical rainforest typical of the Congo basin, the north of the park is characterised by savanna and a mosaic of low-biomass forest types (principally

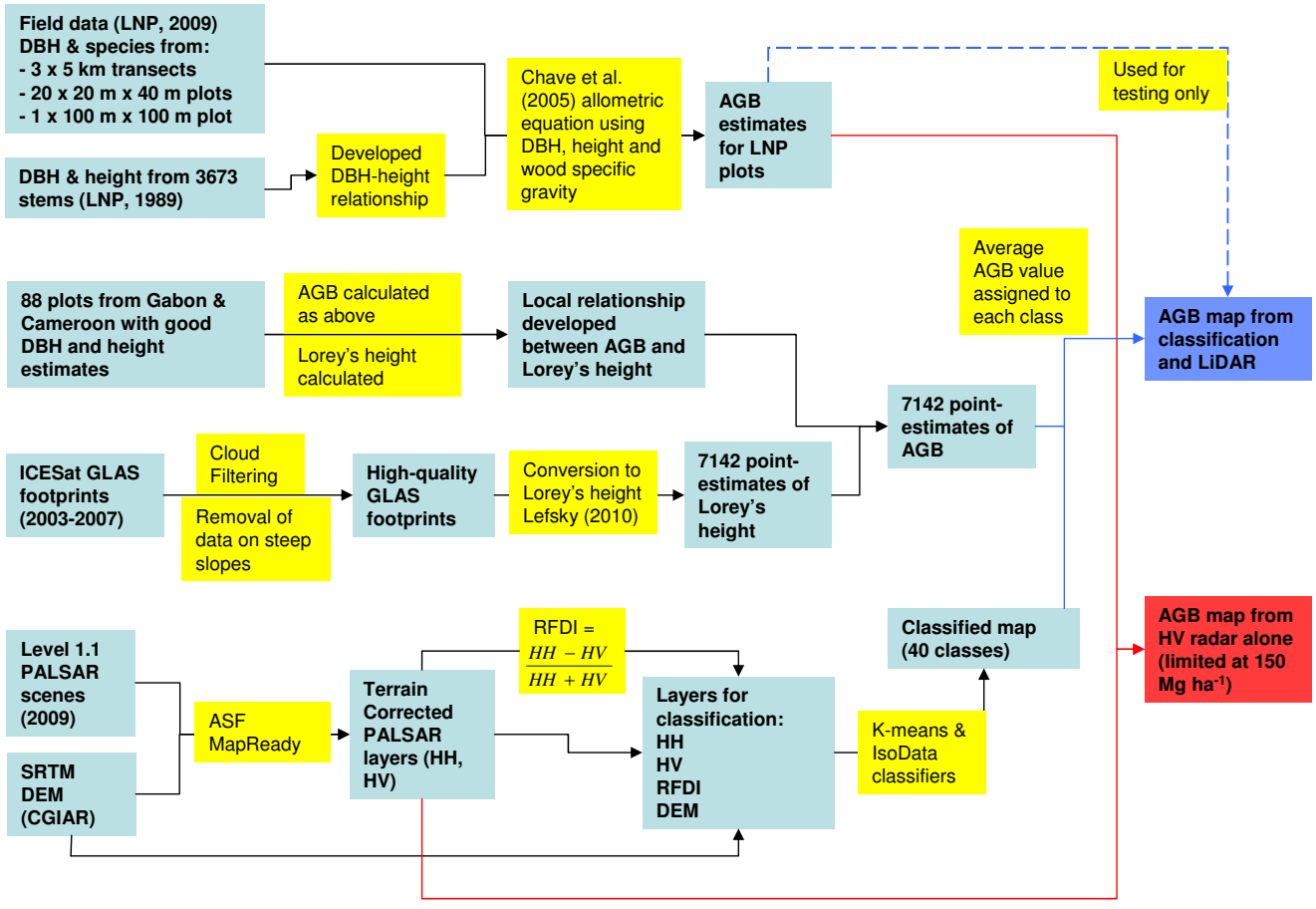

Fig. 2. Diagram showing the processing chain for the production of the biomass maps from the input datasets. AGB = Aboveground Biomass; ASF = Alaska Satellite Facility; CGIAR = Consultative Group on International Agricultural Research; DBH = Diameter at Breast Height (1.3 m); DEM = Digital Elevation Model; ICESat-GLAS = Ice Cloud and land Elevation Satellite – Geoscience Laser Altimeter System; LNP = Lopé National Park; PALSAR = Phased-Array L-band Synthetic Aperture Radar; RFDI = Radar Forest Degradation Index; SRTM = Shuttle Radar Topography Mission.

monodominant Okoumé (*Aucoumea klaineana*) forest, and distinctive open-canopy Marantaceae forest, so-called because the understory is dominated by a thick layer of herbaceous plants of the Marantaceae and Zingiberaceae families). The forest-savanna mosaic is a remnant of the landscape that dominated much of the Congo basin during the Last Glacial Maximum (LGM) (White, 2001). At the LGM savanna covered the majority of LNP, but the increase in precipitation has since caused an expansion of forest to cover nearly the whole area, with forest continuing to expand into the savannas today (White, 2001). Certain forests in the south of the study area may represent Pleistocene refuges that survived through successive glacial maxima that resulted in savanna expansion (Leal, 2001), but much of the northern half of LNP was dominated by savanna until an apparent large reduction in the human population c. 1400 BP (Oslisly and White, 1995). In about 1920 the colonial administration moved all villages from the interior of the LNP, initiating large-scale forest regeneration in previously cultivated zones (Pourtier, 1989). The savanna that remains is maintained by a combination of now limited human burning and the rain-shadow of the Massif du Chaillu, which reduces rainfall to 1500 mm yr^{-1} in the north of the park (White and Abernethy, 1997); whereas rainfall in the south of the park is ~2500 mm yr^{-1} (Tropical Rainfall Measuring Mission (TRMM) 3B43 V6 data January 1998 to January 2010). The site features significant topographic variation and dissection: the altitude ranges from 72 to 980 m a.s.l., and 23.7 % of the study area has a slope great than 20 % (11.3°).

3 Methods

The processing chain is displayed in Fig. 2, and described in the 3.1–3.5 below.

3.1 Field data

A wealth of forestry data has been collected in the LNP since 1983. However, in order to investigate the relationship between radar data and AGB we only used the plots that were re-measured in 2009, which include 3 transects of length 5 km, 20 plots of 20 m × 40 m, and one plot of 100 m × 100 m.

For the 20 × 40 m plots and the 100 m × 100 m plot all stems with a diameter at breast height (DBH) ≥10 cm had their DBH measured and were identified to the species level (or genus if species identification was not possible). The locations of all four corners of each plot were determined using a Garmin 60 CSx GPS. For the 5 km transects all stems ≥ 10 cm DBH were only measured for a 5 m wide band, with stems ≥ 70 cm DBH being measured for a 50 m band. We therefore split each transect into 25 sections of 200 m × 50 m, giving 25 plots of 1 ha size per transect. To calculate AGB values for each 1 ha section of the 50 m wide band, the AGB of the stems between 10 and 70 cm DBH (in the 5 m band) were multiplied by ten and added to the AGB for the ≥ 70 cm stems.

Tree heights were measured in addition to DBH for 3673 stems along the 5 m band of the five transects in 1989. The tree heights were estimated to the nearest meter using a clinometer. These data were used to build a site-specific relationship between tree height and DBH.

AGB was estimated using the moist tropical forest equation from (Chave et al., 2005), involving DBH (D), height (H) and wood specific gravity (ρ):

$$\mathrm{AGB} = 0.0509\left[\rho D^2 H\right] \quad (1)$$

This equation gives AGB in kg dry biomass; throughout this study AGB has been reported in Mg ha^{-1} dry biomass, but where appropriate this has been converted to carbon (Mg C) using the standard conversion factor of 0.5 (IPCC, 2003). Wood specific gravity data were derived from the Global Wood Density database (Chave et al., 2009a; Chave et al., 2009b): species-specific data were available for 64 % of stems, for the rest the average density for members of the genus from tropical Africa were used.

3.2 Lorey's height to AGB relationships

The method used to process the LiDAR data gave an estimate of Lorey's height, a basal-area weighted measure of height (Sect. 3.4). In order to develop a relationship between Lorey's height and AGB, Lorey's height (L) was calculated for each plot using height in metres (H) and basal area in m^2 (A_B, calculated as $\pi(\mathrm{DBH}/2)^2$) for each stem using the following equation:

$$L = \frac{\sum(H \cdot A_B)}{\sum A_B} \quad (2)$$

For calculating Lorey's height from the ground plots we preferred plots for which we had height measurements for every stem – using DBH-height relationships reduces the accuracy of height measurements, and also introduces a spurious correlation as both axes will scale directly with basal area, with only wood density providing the scatter. We therefore used the 5 m band data of the five LNP transects from 1989 (split into 0.25 ha sections, a similar size to the LiDAR footprints, giving 50 plots in total), but this did not give a sufficient number of plots, especially for lower AGB values, to enable us to build up a suitable relationship. To resolve this issue we added the 20 plots of 20 m × 40 m from LNP; though we had to use the DBH-height relationship for these, every stem that was broken off, damaged or deformed was noted in the field notes, reducing errors. We also added plots from nearby areas where DBH and height had been measured for every stem, adding four more 1 ha plots from Gabon (Lewis et al., 2009b), and 14 plots from Mbam Djerem National Park, on the forest-savanna transition zone in Cameroon, which has a similar vegetation type and rainfall to LNP (Mitchard et al., 2011). In total this gave 88 plots where field-measured Lorey's height and AGB could be compared.

3.3 LiDAR data

Space-borne LiDAR data were collected from 2003–2007 over LNP by the Geoscience Laser Altimeter System (GLAS) on the Ice Cloud and Land Elevation Satellite (ICESAT). These data are in the form of circular footprints, with each footprint ranging from 0.2–0.25 ha in size, depending on the terrain slope. In total data for 37 021 individual footprints overlapping with the PALSAR scenes were recorded. However, 26747 of these footprints were removed through cloud filtering, with a further 3132 points removed as they fell on steep slopes (>20 %), where accuracy decreases markedly (Lefsky et al., 2005). This left 7142 GLAS footprints coincident with the six radar scenes (Fig. 1b). Features of the waveforms were correlated with measured Lorey's height from 95 plots in three forest sites in the Amazon, with field plots coincident with GLAS data ($r^2 = 0.83$, RMSE = 3.3 m, $n = 95$), see Lefsky (2010) for details.

3.4 Radar data

Six ALOS PALSAR (Advanced Land Observing Satellite Phased Array L-band SAR) scenes captured on the 25 June 2009 (3 scenes) and 24 July 2009 (3 scenes) were acquired through an ESA (European Space Agency) Category-1 Proposal. These were FBD (Fine-Beam Dual-polarisation) scenes, provided at the 1.1 processing level. We projected the scenes using the Alaska Satellite Facility's software package MapReady 2.3.6. Terrain slope has a significant impact on radar scenes, impacting both the projection of the slant-range image, and the backscatter values, which due to changes in the radar incidence angle are increased on slopes facing

the sensor, and reduced on slopes facing away. To perform the terrain correction we needed a Digital Elevation Model (DEM): we used the 90 m resolution Shuttle Radar Topography Mission (SRTM) dataset, using the void-filled Version 4 product produced by CGIAR-CSI (http://srtm.csi.cgiar.org). We used MapReady to correct geolocation and radiometric problems due to terrain (including adjusting pixel areas due to incidence angle, adjusting backscatter values to account for radar incidence angle, and interpolating layover/shadow regions). The terrain correction was successful, with the topography not visible in the corrected HH and HV images, and there being no residual correlation between the corrected backscatter values and the radar incidence angle.

All processing, including the extraction of radar data values for the field plots, was performed at a 100 m (1 ha) spatial resolution: the same scale as the majority of the field plots (76 out of 96), and a scale at which the heterogeneity of forest structure is normally distributed (Chave et al., 2004), and at which we are confident in our geolocation.

3.5 Unsupervised classification

Due to saturation, direct regression between the field plots data and radar backscatter, as performed for example in Mitchard et al. (2009), was thought to be poorly suited to estimating AGB for LNP, apart from in the small area of savanna in the north. Though we performed the analysis for comparison, it is the LiDAR data that has the potential to estimate the AGB of LNP above the saturation limit of the radar. Rather than averaging the heights of the LiDAR footprints to get an average value for the park, we pursued a solution that would include the spatial information on vegetation structure contained in the radar data.

The Radar Forest Degradation Index (RFDI) (Saatchi et al., 2011) is a ratio between the power of the HH and HV polarisations, designed to assess the strength of the double-bounce term. It is defined as:

$$\mathrm{RFDI} = \frac{\mathrm{HH} - \mathrm{HV}}{\mathrm{HH} + \mathrm{HV}} \quad (3)$$

and picks out this term because HH is sensitive to both volume scattering and double bounce, whereas HV is mostly sensitive to volume scattering. We therefore found it to be a useful layer in helping to differentiate different vegetation types, pulling out more information from the dual-polarisation radar data.

We therefore used the radar backscatter (in HH and HV polarisations), RFDI, and elevation (from the DEM) to develop an unsupervised classification of the park (Fig. 3). We aimed to use as many classes as possible, to enable us to fully characterise the different vegetation structures, and after experimentation we chose 40 classes as this left each class with at least 100 LiDAR observations.

The classification was performed using ENVI 4.7 (ITT Systems), using both the K-means and IsoData unsupervised

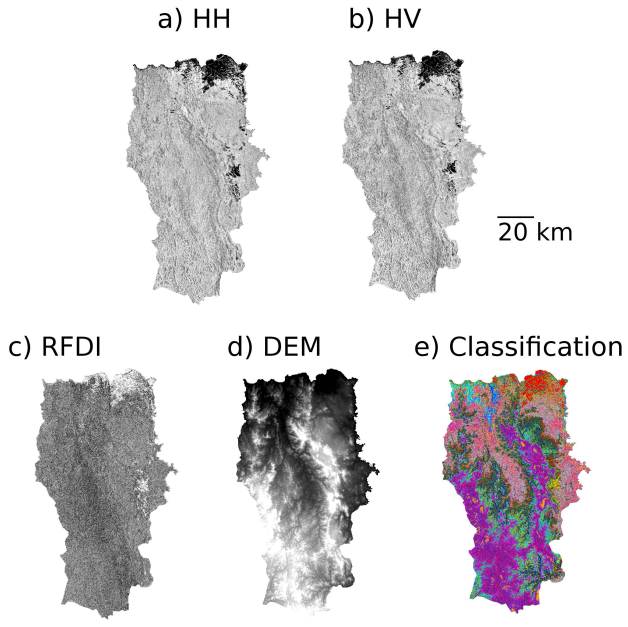

Fig. 3. Images of Lopé National Park using **(a)** PALSAR HH, **(b)** PALSAR HV, **(c)** Radar Forest Degradation Index (RFDI), **(a)** Digital Elevation Model (DEM), **(e)** Classified map, showing 40 classes with arbitrary colours.

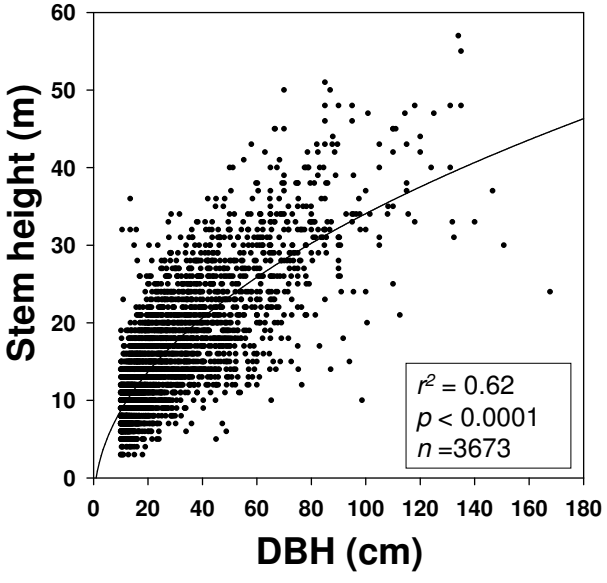

Fig. 4. The relationship between diameter (DBH, cm) and height (m) for 3673 trees measured in 1989 is shown.

Table 1. Coefficients in radar-biomass regressions (± standard errors).

Polaraisation	a	b	c	r^2	p	n
HH	-15.01 ± 1.82	6.85 ± 1.77	-0.012 ± 0.003	0.4	< 0.0001	96
HV	-23.40 ± 2.79	10.00 ± 1.76	-0.017 ± 0.003	0.76	< 0.0001	96

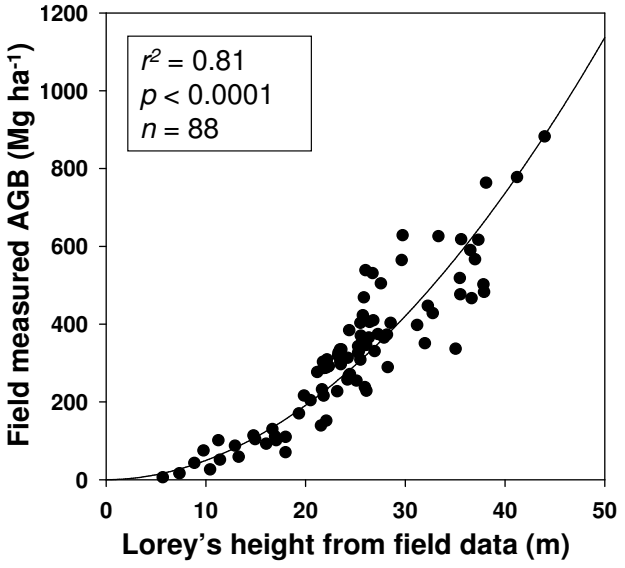

Fig. 5. Field measured AGB for 88 field plots from Lopé in Gabon, nearby plots in Gabon, and Mbam Djerem National Park in Cameroon, plotted against field-measured Lorey's height for these plots. This plot dataset is different to that used for the radar-biomass relationship, as the emphasis here was for plots from the same vegetation-type where every stem was measured, to produce an accurate regression relationship between Lorey's height and AGB.

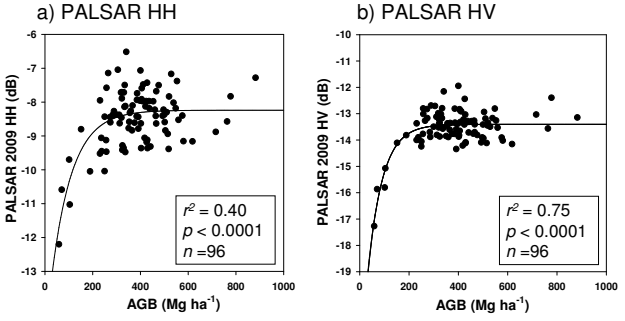

Fig. 6. ALOS PALSAR backscatter in a) HH and b) HV polarisations is plotted against AGB for 96 field plots (including 75×1 ha sections of long transects).

classification methods, with 40 classes and 100 iterations. All four bands (HH, HV, RFDI and DEM height) were scaled to have an identical mean and standard deviation. At this number of iterations both methodologies produced an identical classified map. We then extracted the derived AGB value from each GLAS footprint within each class, averaged these AGB values, and assigned these mean AGB values to each class in order to produce an AGB map.

4 Results

4.1 Stem heights to DBH

We required AGB estimates for the field plots, but though we had DBH and species data for every stem, no stem height data was collected in 2009. Therefore we wished to develop a site-specific relationship between DBH and stem height, based on 3673 stem DBH and heights measured over four transects in 1989. The stem heights (H) were strongly correlated with DBH (D) ($r^2 = 0.62$, $p < 0.0001$, standard error of estimate = 4.97 m, Fig. 4); a second-order regression was chosen because it produced a good fit to the observed data, and is backed up as an appropriate shape by larger datasets (Feldpausch et al., 2011):

$$H = \mathrm{a} + \mathrm{b}\left[D^c\right] \quad (4)$$

with coefficients (± standard errors): $a = -4.25 \pm 1.20$, $b = 4.37 \pm 0.90$, $c = 0.472 \pm 0.037$. This relationship was applied to the stems measured in 2009, allowing AGB to be calculated from the Chave et al. (2005) equation involving DBH, wood density and height.

4.2 Lorey's height to field biomass

We had estimates of Lorey's height from the LiDAR data, but needed to use field plot data to convert these Lorey's height estimates into AGB. To do this we used Lorey's heights (H_L) from the 88 field sites (both from within and near Lopé, and from the Mbam Djerem National Park in Cameroon) where height had been measured for every stem (see Methods). We found that Lorey's height was strongly related to AGB of these plots ($r^2 = 0.81$, $p < 0.0001$, Fig. 5); we treated AGB as the dependent variable here, as it was this that we wished to predict from Lorey's height. The fitted equation was:

$$\mathrm{AGB} = a\left[(H_L)^b\right] \quad (5)$$

with coefficients (± standard errors): $a = 0.564 \pm 0.013, b = 1.945 \pm 0.096$.

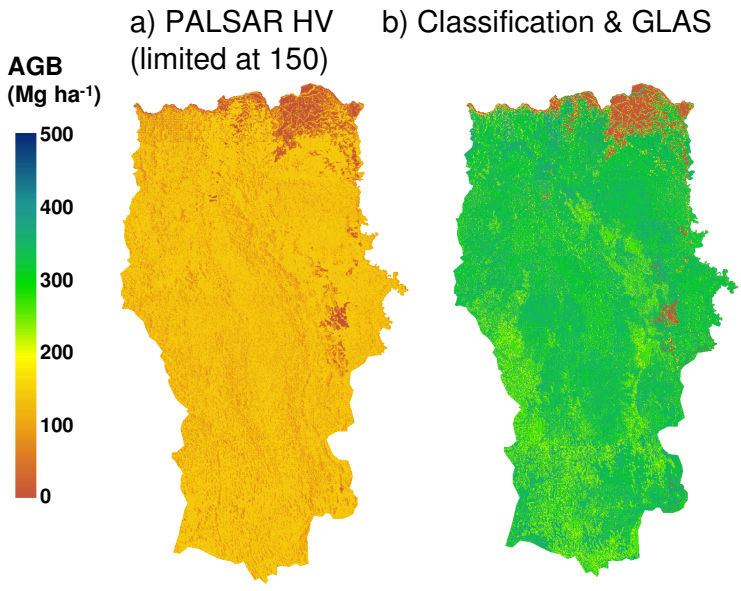

Fig. 7. Two different AGB maps for Lopé national park are displayed. **(a)** is for the regression with PALSAR HV, which is limited at 150 Mg ha^{-1} due to the saturation of these data; **(b)** is for the map produced by classifying PALSAR data and giving the 40 classes AGB values derived from GLAS footprints.

Table 2. Mean LiDAR-derived AGB in broad radar-derived biomass classes.

AGB class from PALSAR HV (Mg ha^{-1})	Mean AGB from LiDAR footrpints within this class (Mg ha^{-1})	Standard Deviation LiDAR-AGB (Mg ha^{-1})	Number of LiDAR footprints
0–25	14.1	13.1	148
25–50	43.1	25.1	131
50–75	68.7	33.8	158
75–100	89.9	35.1	236
100–150	134.4	45.5	1847
> 150	297.2	102.9	4522

4.3 Direct biomass estimation with radar

We then correlated the terrain-corrected radar data (in both the HH and HV polarisations) with the field data. We found a strong relationship with both polarisations, with a saturation point around 100 Mg ha^{-1} for HH, and around 150 Mg ha^{-1} for HV (Fig. 6). The best fit model was the same as that used in Mitchard et al. (2011), also identical in form to the Water Cloud Model (Attema and Ulaby, 1978) (for coefficients see Table 1):

$$\sigma^0_{dB} = a + b[1 - \mathrm{EXP}(c \cdot \mathrm{AGB})] \quad (6)$$

Equation (5) was rearranged as follows to allow the production of an AGB map over the study area using the HV PALSAR data:

$$\mathrm{AGB} = \frac{1}{c} \cdot \ln\left[1 - \frac{\sigma^0_{dB} - a}{b}\right] \quad (7)$$

The relationship between PALSAR HV and AGB saturates at ∼150 Mg ha^{-1} (Fig. 6b, Mitchard et al., 2009, 2011), and thus the map produced was limited at this value (Fig. 7a). Using this upper limit means that using radar data in this way to estimate the AGB of LNP will results in a large underestimation; however for comparison, and as an absolute lower limit, this methodology estimates the aboveground biomass of LNP to be 67.5 Tg, equivalent to 33.7 Tg C (Fig. 7a).

4.4 Classification and mapping by GLAS

A K-means and IsoData classification with 40 classes and 100 iterations were found to give identical results, and a classification that, based on our field knowledge, classified separately and accurately all the major vegetation types. No more than 40 classes were used, as experimentation showed that more would have resulted in fewer than 100 GLAS footprints falling within each class.

Table 3. Comparison of mean AGB for classes from LiDAR with mean AGB from field plots found within these classes.

Class number	Class mean AGB (from GLAS) ($Mg\,ha^{-1}$)	Mean AGB field plots ($Mg\,ha^{-1}$)	Standard Deviation of field plots ($Mg\,ha^{-1}$)	Number field plots in class
14	296.1	305.2	44.6	5
5	313.0	310.0	82.1	5
9	314.5	271.6	109.0	13
15	325.6	359.9	74.5	8
12	337.3	370.0	163.8	16
23	338.5	405.3	52.4	6
28	347.7	363.9	111.2	11
18	366.1	320.7	90.7	5
11	393.0	453.6	152.7	8
20	421.1	458.9	95.0	4
Mean	345.3	361.9	97.6	8.1

Each class was given an average AGB value by converting each GLAS footprint into an AGB estimate (Eq. 4), then averaging these AGB estimates within each class. This gives a carbon stock estimate for LNP of 156 Tg biomass, 78 Tg C (Fig. 7b). It gives the average AGB as $315\,Mg\,ha^{-1}$, which compares much better to the field plots and LiDAR data-derived averages (390 and $251\,Mg\,ha^{-1}$ respectively) than the $136\,Mg\,ha^{-1}$ from the (limited at $150\,Mg\,ha^{-1}$) PALSAR HV-derived map.

4.5 Comparisons with independent data

The LiDAR data were not used in the creation of the radar-based AGB map, and similarly the field data were not used to create the classification-based map. This allows a test of the accuracy of both approaches using independent data.

4.5.1 Comparison of radar-derived AGB map to LiDAR data

Due to geolocation errors and differences in scale a direct comparison between the 100 m AGB pixels and the 0.2–0.25 ha GLAS footprints would not give an appropriate estimation of error; even with a perfect AGB map there would be a lot of scatter in the result. Instead the HV-derived AGB map was divided into 6 classes (0–25, 25–50, 50–75, 75–100, 100–150, and $>150\,Mg\,ha^{-1}$), and the mean and standard deviation of the LiDAR-derived AGB values in each class compared (Table 2). The mean of the LiDAR-derived AGB values for each class fall within that class, suggesting the PALSAR HV-derived map is producing consistent, unbiased results throughout its sensitivity range.

4.5.2 Comparison of LiDAR and classification-derived AGB map to field data

We do not have access to a sufficient number of field plots to enable the use of these to confirm the accuracy of all 40 classes. However, ten of the classes, covering 34.7 % of LNP in total, had four or more field plots located within them. The mean of these field plots were an average of 9.5 % (range: 1–16 %) different from the mean AGB derived from the GLAS data (Table 3). These data provide evidence of a small bias, with the average AGB values for the field data being on average 4.5 % higher than the mean value for the class derived from LiDAR data.

5 Error estimation

When providing estimates of carbon stocks for REDD+ and other carbon forestry projects, an estimate is useless without an associated estimate of accuracy. Normally the number of carbon assets awarded is based on the most conservative estimate (e.g. the lower boundary of a 95 % confidence interval about the mean) (Grassi et al., 2008; GOFC-GOLD, 2009). The results in Sect. 4.5 provide some confidence in our methodologies, but due to the limited number and spatial distribution of the field plots, and the inaccuracies inherent in LiDAR-AGB estimation, these do not provide an estimate of the true error of the analysis.

The uncertainty of any measurement can be divided into two components: that of accuracy and precision (IPCC, 2000). Accuracy is the distance of the mean (of many observations) the true value: it is thus influenced by biases (consistent errors) in the estimation process. It is this parameter that we are principally interested in here. The other component, precision, relates to how close an individual measurement is to the mean value of many measurements of the same parameter: in other words it is related to random errors. These random errors are caused by spatial and structural heterogeneity, geolocation errors, changes in vegetation between observations, and measurement error, and are responsible for much of the noise observable in Figs. 4–6, and the differences between field plot averages and the GLAS-averages of

their classes reported in Sect. 4.5.2 and Table 3. It is not as important to quantify the degree of precision for our purposes here (calculating carbon stocks over a large area), as these random errors will cancel out over the very large number of measurements. However, the precision is important when measuring changes at a pixel level: therefore for any methodology that wishes to assess change precision is very important (see Mitchard et al., 2011). But precision will be discussed no further in this section, as it does not affect the uncertainty of the AGB estimate for the whole park: we are interested here only in accuracy, and thus in trying to estimate the magnitude of potential degree of biases throughout the stages of our estimation process.

5.1 Uncertainties in the LiDAR-classification map

a. Allometric equations: the AGB values derived from both the field and LiDAR data are ultimately derived from measurements of the diameter, height and species of trees. These are converted to AGB for this study using the Chave et al. (2005) equations, which while believed to be the best available, have significant, but hard to estimate, uncertainties. They are not derived from African trees, which may be a problem as there are known to be differences in height-DBH relationships between the continents (Feldpausch et al., 2010); however our use of a locally-derived DBH-height relationship should correct for this, and Lewis et al. (2009) showed that locally-derived relationships did not dramatically alter their biomass estimates from African forests (Lewis et al., 2009b). We therefore estimate the potential bias due to the allometric equation at $\pm 10\,\%$ (at the 95 % confidence level), which though twice the figure published in the original paper with this equation (Chave et al., 2005), is similar to that discovered by Lewis et al. (2009), who propagated estimated height and diameter errors in their biomass estimates, and by Djomo et al. (2010), who used destructive sampling of trees in Africa to estimate the accuracy of various pantropical equations.

b. LiDAR waveform to Lorey's height: the relationship used to derive Lorey's height from the LiDAR waveforms is based on field plots coincident with LiDAR footprints from three sites in the Brazilian Amazon (Lefsky, 2010). Unfortunately no LiDAR footprints intersected with our field plots from LNP, so we cannot discern the extent to which this could cause inaccuracies, though the results in Section 4.5 provide some confidence. There are structural differences between the two continents' forests (Djomo et al., 2010), so we add an uncertainty of $\pm 5\,\%$, similar in magnitude to the detected potential bias in Sect. 4.5.2, to account for this.

c. Classification: classifying the image into forty different clusters, based on similar radar returns and elevation, is bound to introduce errors by both over-simplification (the resulting vegetation types will not necessarily have identical average AGB values in different spatial locations) and mis-classification. As the clusters are only covered by LiDAR data from a spatially-limited portion of the image (Fig. 1b), this is likely to introduce biases. To test this we ran four additional models, excluding LiDAR data from one quarter of the park each time, and comparing the biomass results produced from that quarter with the original biomass estimates. This resulted in changes in the biomass estimate for each quarter of 4.8 % (range $4 - 7\,\%$). This procedure only estimates part of the potential error due to this source, so to be conservative we add an error of ± 10 %.

5.2 Summing uncertainties

As these errors are all independent and not necessarily normally distributed about the mean, the most conservative method of error summing should be used, namely that these errors should be summed to give an estimate of the most extreme error (Eq. A1.1, Page A.16, IPCC, 2000): this is $\pm 25\,\%$. This gives the total AGB stocks of LNP, using the LiDAR data and unsupervised classification methodology, to be between 58.5 and 97.5 Tg C. Though the most likely carbon stock of LNP is the mean, 78 Tg C, for the purposes of REDD+ or similar systems the lower bound, 58.5 Tg C, may be preferred (Grassi et al., 2008), as we have confidence that the true carbon stock is at least as high as this value.

6 Discussion

Despite the high biomass and persistent cloud-cover, we have produced a high resolution (100 m) map of AGB over Lopé National Park in Gabon. This estimate was made possible through a novel fusion of radar and spaceborne LiDAR data. Also, using a conservative error-estimation method optimised for carbon payments for REDD+, we have shown that these estimates at a park level have a $\pm 25\,\%$ uncertainty, due to potential biased errors in our input data and estimations. We have shown from our field data that there is a strong relationship between Lorey's height and field-derived AGB, and then used this to give us an additional 7042 point-based AGB estimates from spaceborne LiDAR waveforms, which can estimate Lorey's height with high confidence (Lefsky, 2010). Finally we used the information in our dual-polarisation radar data, along with a DEM, to classify the vegetation into units with distinct biophysical parameters, enabling the spatial extrapolation of the radar data. While none of these steps are novel or controversial, we believe this new combination of methodologies provides an excellent pathway for combining the strengths of GLAS and radar data to produce AGB maps of high biomass forest.

This methodology enables the production of carbon maps for a tropical region or country, a requirement, for example,

in advance of a deforestation-reduction program such as REDD+. However, the high resolution and spatially-explicit nature of these maps goes beyond the requirements of the lower two assessment standards given by the International Panel on Climate Change (IPCC), which rely on maps giving changes in landcover type and not on spatially-explicit AGB maps. Therefore using such a methodology could give data required for the highest tier, Tier 3 (GOFC-GOLD, 2009). Running Tier 3 assessments may be advantageous, as the increased certainty may lead to a larger number of certified emissions reductions for a landscape. Additionally, Tier 3 monitoring may increase investor confidence leading to increased investments in REDD+. Furthermore, such monitoring may lead to this carbon being trade at a price premium if the REDD+ scheme moves to become a market-based scheme. The method developed here shows that a large investment in a high density of field plots or airborne LiDAR data may not be necessary to reach the accuracy required by this tier: a high density of GLAS plots, combined with optical or radar data for vegetation classification, may suffice, as long as there are sufficient field plots for validation.

Our approach to the uncertainty analysis, using conservative estimates of potential biases from a wide variety of sources, and then summing them, is conservative, but appropriate to the problem in hand. For such a large area it will produce much wider confidence intervals than commonly used estimates based on standard errors of means, but this is appropriate as for the purposes of conserving carbon stocks we must find the minimum likely carbon stocks of the park, not a mean estimate. One limitation is the necessity of estimating many of the uncertainty parameters, as no hard data exists, and thus the uncertainty estimates are themselves uncertain: however this does not reduce the importance of making such estimates. We believe this approach is essential for the monitoring of biomass, where the conservativeness principle outlined by Grassi et al. (2008), that for the purposes of forest conservation the most conservative estimate of any parameter must always be used, must apply. This conservative approach is essential for two reasons. Firstly, if avoided deforestation credits are to be used to offset actual fossil fuel carbon emissions, then any overestimate of carbon savings realised would result in REDD+ have a net negative impact on net CO_2 emissions, exactly the opposite of its original intentions. Secondly, the majority of the errors included in our analysis are very hard to quantify, that is these uncertainties are themselves very uncertain. Therefore our conservative approach assists in ensuring that the confidence bands presented span the full range of possible values.

GLAS-LiDAR is clearly not the ideal tool for mapping biomass: its footprints cover only a tiny percentage of the total land-area of the planet, and the footprints, at 0.2–0.25 ha, are too large for detailed mapping. It would always be preferable to use airborne LiDAR, as for example Asner et al. (2010) have done in the Peruvian Amazon, using a similar approach as described here but with airborne-LiDAR, extrapolated to other areas using the classification of high-resolution optical rather than radar data. However, airborne LiDAR data is expensive to collect, thus whole country censuses, let alone with annual repeat, are unlikely in the near future. GLAS represents a spatially distributed set of footprints, with hundreds of thousands to millions of footprints freely available across every country (Lefsky, 2010), and as such is a useful resource to assist mapping forest biomass carbon stocks. The patchy coverage necessitates using another dataset to classify the landscape: here we use radar data and a DEM due to data availability, but if cloud-free optical data (or other high quality spatially-explicit datasets) were available they should be added into the classification procedure.

A limitation with the approach we set out here is that IceSAT GLAS is no longer operational: suitable data were only produced from 2003 until 2009. A new satellite carrying a spaceborne LiDAR system, ICESat-2, is planned for launch in late 2015 (http://icesat.gsfc.nasa.gov/icesat2/). Unlike ICESat, ICESat-2 will use a micropulse multi-beam approach, which will produce a greater number of smaller footprints, with great potential for biomass retrieval; however, this new approach will necessitate new algorithm development and testing. The lack of data from 2009–2015 will mean that though this method may be used to produce carbon maps for the mid- to late- 2000s, it will not be possible to use this for change detection or deforestation monitoring in the near future. However this is still a useful development: both optical and radar systems can easily be used to detect changes in forest *area*, and so having an accurate carbon map at one time-point will allow the emissions caused by deforestation to be better estimated from landcover-change results.

Acknowledgements. This work is dedicated to the memory of Fabiane Lima de Oliveira, who passed away in Gabon in 2009 after falling ill whilst on fieldwork for this project. Her deep knowledge and love of the forest was highly respected by all who she met. She is greatly missed by family, friends and the scientific community. ESA provided the ALOS PALSAR radar data at cost price through a Category 1 Application. These data were ultimately collected and processed by JAXA. ICESat GLAS data were provided by NASA. SRTM data were provided by NASA and processed by CGIAR-CSI (http://srtm.csi.cgiar.org). Funding for this work was provided by a Gatsby Plants PhD Studentship fo Edward Mitchard, with the fieldwork being funded by a grant from the Gordon and Betty Moore Foundation and the Packard Foundation. Simon Lewis is supported by a Royal Society University Research Fellowship. The Gabonese Agence Nationale des Parcs Nationaux, the Station d'Etudes des Gorilles et Chimpanzés, and Etienne Massard provided essential logistical support to the fieldwork effort.

Edited by: K. Thonicke

References

Abdalati, W., Zwally, H. J., Bindschadler, R., Csatho, B., Farrell, S. L., Fricker, H. A., Harding, D., Kwok, R., Lefsky, M., Markus, T., Marshak, A., Neumann, T., Palm, S., Schutz, B., Smith, B., Spinhirne, J., and Webb, C.: The ICESat-2 Laser Altimetry Mission, Proc. IEEE, 98, 735–751, 2010.

Ahrends, A., Burgess, N. D., Milledge, S. A. H., Bulling, M. T., Fisher, B., Smart, J. C. R., Clarke, G. P., Mhoro, B. E., and Lewis, S. L.: Predictable waves of sequential forest degradation and biodiversity loss spreading from an African city, P. Natl. Acad. Sci. USA, 107, 14556–14561, 2010.

Asner, G. P., Powell, G. V. N., Mascaro, J., Knapp, D. E., Clark, J. K., Jacobson, J., Kennedy-Bowdoin, T., Balaji, A., Paez-Acosta, G., Victoria, E., Secada, L., Valqui, M., and Hughes, R. F.: High-resolution forest carbon stocks and emissions in the Amazon, P. Natl. Acad. Sci. USA, 107, 16738–16742, 2010.

Attema, E. P. W. and Ulaby, F. T.: Vegetation Modeled as a Water Cloud, Radio Sci., 13, 357–364, 1978.

Brown, S.: Estimating Biomass and Biomass Change of Tropical Forests, FAO Forest Paper 134, Rome, 1997.

CCBA: List of accepted CCBA projects, http://www.climate-standards.org/projects/index.html, 2011.

Chave, J., Condit, R., Aguilar, S., Hernandez, A., Lao, S., and Perez, R.: Error propagation and scaling for tropical forest biomass estimates, Philos. T. R. Soc. Lon. B, 359, 409–420, 2004.

Chave, J., Andalo, C., Brown, S., Cairns, M. A., Chambers, J. Q., Eamus, D., Folster, H., Fromard, F., Higuchi, N., Kira, T., Lescure, J. P., Nelson, B. W., Ogawa, H., Puig, H., Riera, B., and Yamakura, T.: Tree allometry and improved estimation of carbon stocks and balance in tropical forests, Oecologia, 145, 87–99, 2005.

Chave, J., Coomes, D., Jansen, S., Lewis, S. L., Swenson, N. G., and Zanne, A. E.: Towards a worldwide wood economics spectrum, Ecol. Lett., 12, 351–366, 2009b.

Chhatre, A. and Agrawal, A.: Forest commons and local enforcement, P. Natl. Acad. Sci. USA, 105, 13286–13291, 2008.

Chhatre, A. and Agrawal, A.: Trade-offs and synergies between carbon storage and livelihood benefits from forest commons, P. Natl. Acad. Sci. USA, 106, 17667–17670, 2009.

Clements, G. R., Sayer, J., Boedhihartono, A. K., Venter, O., Lovejoy, T., Koh, L. P., and Laurance, W. F.: Cautious Optimism over Norway-Indonesia REDD Pact, Conserv. Biol., 24, 1437–1438, 2010.

Clements, T.: Reduced Expectations: the political and institutional challenges of REDD, Oryx, 44, 309–310, 2010.

Djomo, A. N., Ibrahima, A., Saborowski, J., and Gravenhorst, G.: Allometric equations for biomass estimations in Cameroon and pan moist tropical equations including biomass data from Africa, Forest. Ecol. Manag., 260, 1873–1885, 2010.

Donnellan, A., Rosen, P., Graf, J., Loverro, A., Freeman, A., Treuhaft, R., Oberto, R., Simard, M., Rignot, E., Kwok, R., Pi, X. P., Blair, J. B., Abdalati, W., Ranson, J., Zebker, H., Hager, B., Shugart, H., Fahnestock, M., and Dubayah, R.: Deformation, Ecosystem Structure, and Engel, S., Pagiola, S., and Wunder, S.: Designing payments for environmental services in theory and practice: An overview of the issues, Payments for Environmental Services in Developing and Developed Countries, 65, 663–674, 2008.

Feldpausch, T. R., Banin, L., Phillips, O. L., Baker, T. R., Lewis, S. L., Quesada, C. A., Affum-Baffoe, K., Arets, E. J. M. M., Berry, N. J., Bird, M., Brondizio, E. S., de Camargo, P., Chave, J., Djagbletey, G., Domingues, T. F., Drescher, M., Fearnside, P. M., Frana, M. B., Fyllas, N. M., Lopez-Gonzalez, G., Hladik, A., Higuchi, N., Hunter, M. O., Iida, Y., Abu Silam, K., Kassim, A. R., Keller, M., Kemp, J., King, D. A., Lovett, J. C., Marimon, B. S., Marimon-Junior, B. H., Lenza, E., Marshall, A. R., Metcalfe, D. J., Mitchard, E. T. A., Moran, E. F., Nelson, B. W., Nilus, R., Nogueira, E. M., Palace, M., Patiño, S., Peh, K. S.-H., Raventos, M. T., Reitsma, J. M., Saiz, G., Schrodt, F., Sonké, B., Taedoumg, H. E., Tan, S., White, L., Wöll, H., and Lloyd, J.: Height-diameter allometry of tropical forest trees, Biogeosciences Discuss., 7, 7727–7793, doi:10.5194/bgd-7-7727-2010, 2010.

Geist, H. J. and Lambin, E. F.: Proximate causes and underlying driving forces of tropical deforestation, Bioscience, 52, 143–150, 2002.

GOFC-GOLD: A sourcebook of methods and procedures for monitoring and reporting anthropogenic greenhouse has emissions and removals caused by deforestation, gains and losses of carbon stocks in forests, remaining forests, and forestation, Alberta, Canada, 2009.

Grassi, G., Monni, S., Federici, S., Achard, F., and Mollicone, D.: Applying the conservativeness principle to REDD to deal with the uncertainties of the estimates, Environ. Res. Lett., 3, 035005, 2008.

IPCC: Good Practice Guidance and Uncertainty Management in National Greenhouse Gas Inventories, IPCC, 2000.

IPCC: Good practice guidance for land use, land-use change and forestry, IPCC, 2003.

Kaiser, B. and Roumasset, J.: Valuing indirect ecosystem services: the case of tropical watersheds, Environ. Dev. Econ., 7, 701–714, 2002.

Leal, M. E.: Microrefugia, Small Scale Ice Age Forest Remnants, Systematics and Geography of Plants, 71, 1073–1077, 2001.

Lefsky, M.: A global forest canopy height map from the Moderate Resolution Imaging Spectroradiometer and the Geoscience Laser Altimeter System, Geophys. Res. Lett., 37, L15401, doi:10.1029/2010GL043622, 2010.

Lefsky, M. A., Harding, D. J., Keller, M., Cohen, W. B., Carabajal, C. C., Espirito-Santo, F. D., Hunter, M. O., and de Oliveira, R.: Estimates of forest canopy height and aboveground biomass using ICESat, Geophys. Res. Lett., 32, L22S02, doi:10.1029/2005GL023971, 2005.

Lewis, S. L., Lloyd, J., Sitch, S., Mitchard, E. T. A., and Laurance, W. F.: Changing Ecology of Tropical Forests: Evidence and Drivers, Annu. Rev. Ecol. Evol. Systemat., 40, 529–549, 2009a.

Lewis, S. L., Lopez-Gonzalez, G., Sonke, B., Affum-Baffoe, K., Baker, T. R., Ojo, L. O., Phillips, O. L., Reitsma, J. M., White, L., Comiskey, J. A., Djuikouo, M. N., Ewango, C. E. N., Feldpausch, T. R., Hamilton, A. C., Gloor, M., Hart, T., Hladik, A., Lloyd, J., Lovett, J. C., Makana, J. R., Malhi, Y., Mbago, F. M., Ndangalasi, H. J., Peacock, J., Peh, K. S. H., Sheil, D., Sunderland, T., Swaine, M. D., Taplin, J., Taylor, D., Thomas, S. C., Votere, R., and Woll, H.: Increasing carbon storage in intact African tropical forests, Nature, 457, 1003–1006, 2009b.

Lu, D. S.: The potential and challenge of remote sensing-based biomass estimation, Int. J. Remote Sens., 27, 1297–1328, 2006.

Mayaux, P., Bartholome, E., Fritz, S., and Belward, A.: A new land-cover map of Africa for the year 2000, J. Biogeogr., 31, 861–877, 2004.

Meir, P., Cox, P., and Grace, J.: The influence of terrestrial ecosystems on climate, Trends Ecol. Evol., 21, 254–260, 2006.

Mitchard, E. T. A., Saatchi, S. S., Woodhouse, I. H., Nangendo, G., Ribeiro, N. S., Williams, M., Ryan, C. M., Lewis, S. L., Feldpausch, T. R., and Meir, P.: Using satellite radar backscatter to predict above-ground woody biomass: A consistent relationship across four different African landscapes, Geophys. Res. Lett., 36, L23401, doi:10.1029/2009GL040692, 2009.

Mitchard, E. T. A., Saatchi, S., Woodhouse, I., Feldpausch, T., Lewis, S., Sonké, B., Rowland, C., and Meir, P.: Measuring biomass changes due to woody encroachment and deforestation/degradation in a forest-savanna boundary region of central Africa using multi-temporal L-band radar backscatter, Remote Sens. Environ., 115, 2861–2873, 2011.

Oslisly, R. and White, L. J. T.: La relation homme-milieu dans la reserve de la Lopé (Gabon) au cours de l'Holocène; les implications sur l'environnement., in: Dynamique à long terme des Ecosystèmes Forestiers Intertropicaux, edited by: Servant, M., and Servant-Vildary, S., ORSTOM, 241–250, 1995.

Phillips, O. L., Lewis, S. L., Baker, T. R., Chao, K. J., and Higuchi, N.: The changing Amazon forest, Philos. T. Roy. Soc. B., 363, 1819–1827, 2008.

RAINFOR: Field manual for plot establishment and remeasurement, http://www.geog.leeds.ac.uk/projects/rainfor/, last access: 10 January 2011, 2009.

Pourtier, R.: Le Gabon. Tome 2: Etat et Développement., Editions L'Harmattan, Paris, France, 1989.

Rodrigues, A. S. L., Ewers, R. M., Parry, L., Souza, C., Verissimo, A., and Balmford, A.: Boom-and-Bust Development Patterns Across the Amazon Deforestation Frontier, Science, 324, 1435–1437, 2009.

Shugart, H. H., Saatchi, S., and Hall, F. G.: Importance of structure and its measurement in quantifying function of forest ecosystems, J. Geophys. Res., 115, G00E13, doi:10.1029/2009JG000993, 2010.

Stern, N. H.: The economics of climate change: the Stern review, Cambridge University Press, Cambridge, xix, 692 pp., 2008.

Swetnam, T., Falk, D. A., Hessl, A. E., and Farris, C.: Reconstructing landscape patter of historical fires and fire regimes, in: The lanscape ecology of fire, edited by: McKenzie, D., Miller, C., and Falk, D. A., Springer, Ecological Studies, 213, 165–192, 2011.

White, L. J. T.: Forest-savanna dynamics and the origins of 'Marantaceae Forest' in the Lopé Reserve, Gabon, in: African Rain Forest Ecology and Conservation, edited by: Weber, B., White, L. J. T., and Vedder, A., Yale University Press, 165–192, 2001.

White, L. J. T. and Abernethy, K.: A guide to the vegetation of the Lopé Reserve, Wildlife Conservation Society, New York, USA, 1997.

WRI: Summary of Developed Country "Fast-Start" Climate Finance Pledges, World Resources Institute, 2010.